Open access • Posted Content • DOI:10.1101/2021.06.04.447102

# Microstructural development across white matter from 9-13 years — Source link

Clare E. Palmer, Diliana Pecheva, John R. Iversen, Donald J. Hagler ...+6 more authors

**Institutions:** University of California, Berkeley, University of California, San Diego

**Published on:** 06 Jun 2021 - bioRxiv (Cold Spring Harbor Laboratory)

**Topics:** Diffusion MRI

# Microstructural development across white matter from 9-13 years

C E Palmer[1], D Pecheva[2,3], J Iversen[2], DJ Hagler Jr[2,3], L Sugrue[4], P Nedelec[4], C Fan[2], W K Thompson[5], T L Jernigan*[1,3,6,7]& A M Dale*[2,3,6,8,]

1. Center for Human Development, University of California, San Diego, 9500 Gilman Drive, La Jolla, CA 92161, USA
2. Center for Multimodal Imaging and Genetics, University of California, San Diego School of Medicine, 9444 Medical Center Dr, La Jolla, CA 92037, USA
3. Department of Radiology, University of California, San Diego School of Medicine, 9500 Gilman Drive, La Jolla, CA 92037, USA
4. Department of Radiology and Biomedical Imaging, University of California, San Francisco, 505 Parnassus Avenue, San Francisco, CA 94143, USA
5. Division of Biostatistics, Department of Family Medicine and Public Health, University of California, San Diego, La Jolla, CA, USA
6. Department of Cognitive Science, University of California, San Diego, 9500 Gilman Drive, La Jolla, CA 92161, USA
7. Department of Psychiatry, University of California, San Diego School of Medicine, 9500 Gilman Drive, La Jolla, CA 92037, USA
8. Department of Neuroscience, University of California, San Diego School of Medicine, 9500 Gilman Drive, La Jolla, CA 92037, USA

*These authors contributed equally.

Corresponding author: Dr. Clare E Palmer (cepalmer@ucsd.edu), Center for Human Development, University of California, San Diego, 9500 Gilman Drive, La Jolla, CA 92161, USA

Keywords: development, neuroimaging, microstructure, white matter, adolescence, diffusion

# ABSTRACT

Development in late childhood has been associated with microstructural changes in white matter (WM) that are hypothesized to underpin concurrent changes in cognitive and behavioral function. Restriction spectrum imaging (RSI) is a framework for modelling diffusion-weighted imaging that can probe microstructural changes within hindered and restricted compartments providing greater specificity than diffusion tensor imaging for characterizing intracellular diffusion. Using RSI, we modelled voxelwise restricted isotropic, N0, and anisotropic, ND, diffusion across the brain and measured cross-sectional and longitudinal age associations in a large sample (n=8,039) aged 9-13 years from the Adolescent Brain and Cognitive Development (ABCD) Study[SM]. Participants showed global increases in N0 and ND across WM with age. When controlling for global RSI measures (averaged across WM), we found smaller age-related associations in frontal regions, reflective of more protracted development of frontal WM. Moreover, variability in the development of restricted diffusion in subcortical regions and along particular gray-white matter boundaries was independent of the global developmental effect. Using the ABCD sample, we have unprecedented statistical power to estimate developmental effects with high precision. Our analyses reveal spatially-varying maturational changes for different regions, independent of global changes. This non-uniformity may reflect age-dependent development of distinct cognitive and behavioral processes.

# INTRODUCTION

Throughout childhood and adolescence cerebral white matter (WM) undergoes substantial microstructural changes. WM tracts connect distributed neural networks across the brain that are essential for a multitude of cognitive functions that continue to develop into late childhood (Baron Nelson et al., 2019; Peters et al., 2012; Simmonds et al., 2014). Diffusion tensor imaging (DTI) has been used to examine WM microstructural development. Several studies have shown increases in fractional anisotropy (FA) and decreases in mean diffusivity (MD) throughout the brain across childhood and into young adulthood (review Lebel& Deoni, 2018, Lebel et al, 2019), with developmental trajectories shown to differ by region over large age ranges (Krogsrud et al., 2016a; Catherine Lebel & Beaulieu, 2011a; Pohl et al., 2016). These microstructural changes have been associated with decreased radial diffusivity (diffusion in the perpendicular axis), which is thought to reflect increases in axonal packing and/or myelination (Beaulieu, 2002; Song et al., 2005).

However, many developmental studies of microstructure in the WM are cross-sectional and with small sample sizes. In the current study, we analyzed longitudinal data across two time points from the Adolescent Brain and Cognitive Development (ABCD) Study (n=8039; 9-13 years) in order to estimate developmental changes in tissue microstructure across the WM. We modeled both baseline age ($age_0$) and change in age from baseline to follow-up ($age_\Delta$) in order to delineate cross-sectional and longitudinal developmental effects (Morrell et al., 2009; Sørensen et al., 2021). The cross-sectional effects estimate variability in our diffusion metrics with age across all individuals at a given point in time; whereas, the longitudinal effects estimate how the brain changes with increasing age within subjects with multiple time points. A difference in the model estimates for these predictors may indicate non-linear age effects from 9-13 years old or differences in participants within the cohort that have one vs multiple imaging scans, which may be particularly pertinent in the current study where only half of the cohort (disproportionately those who were recruited earlier) have two imaging scans.

Many previous studies have focused on developmental associations with DTI metrics, but only more recent studies have started using more advanced data acquisition protocols and models of diffusion (Genc, Malpas, et al., 2017; Lynch et al., 2020; Mah et al., 2017). The use of multiple b-values and high angular resolution diffusion imaging (HARDI) has enabled more complex models of tissue microstructure, taking into account multiple tissue compartments, such as multiple fiber populations in WM and orientated structure of neurites within grey matter. This is important because the diffusion tensor model only allows the expression of a single principal direction of diffusion and is unable to characterize mixtures of neurite orientations within a voxel. In the current study, we employ restriction spectrum imaging (RSI; Brunsing et al., 2017; White et al., 2013, 2014), which uses multiple b-value HARDI data to decompose the diffusion-weighted signal into different components emanating from multiple compartments with different diffusion properties, for example free water, hindered and restricted compartments. Palmer et al (2021) provides an in-depth description of these different environments and the biological processes that can contribute to changes in diffusion within these

compartments. Importantly, the hindered compartment primarily represents diffusion in the extracellular space, although may also describe diffusion within intracellular spaces with dimensions larger than the diffusion length scale (typically, ~10μm, for the diffusion sequences used in human imaging studies); and the restricted compartment primarily represents diffusion in the intracellular space, within cells or processes of dimensions smaller than the diffusion length scale. Free water diffusion primarily represents water within CSF or intravascular spaces. Within each voxel, RSI models the diffusion signal as a linear mixture of these different compartments. For the restricted compartment, spherical harmonic (SH) coefficients are used to estimate the relative signal fraction of restricted anisotropic (directional) diffusion (ND) and the restricted isotropic (zeroth order) diffusion (N0). Using this model, we can more precisely understand the underlying microstructural developmental changes occurring in late childhood and adolescence.

Although RSI has not previously been used to study developmental changes in WM in late childhood, similar multi-compartment models, such as neurite orientation dispersion and density imaging (NODDI), have been shown to be more sensitive to developmental changes than DTI metrics (Genc, Malpas, et al., 2017). Neurite density index (NDI), which reflects the intracellular volume fraction, was positively associated with age across all WM tracts in several recent studies (Geeraert et al., 2019; Genc, Malpas, et al., 2017; Lynch et al., 2020; Mah et al., 2017). However, the orientation dispersion index (ODI), a measure of the degree of dispersion of intracellular diffusion, showed no age associations, suggesting that WM development across childhood and adolescence was not associated with changes in axon coherence (Genc, Malpas, et al., 2017; Lynch et al., 2020). Although NODDI is a useful model for describing intracellular diffusion, NDI is limited in that it presents a measure of the total intracellular volume fraction; in contrast, RSI uses spherical deconvolution to reconstruct the fiber orientation distribution (FOD) in each voxel for each compartment, in order to delineate isotropic and anisotropic diffusion. Moreover, in voxels with crossing fibers that are oriented perpendicular to one another, ODI will be estimated to be very high; whereas ND, from RSI, will provide a more accurate estimation of the anisotropy of the two coherent crossing fibers. RSI therefore provides differential information about the intracellular diffusion within each voxel compared to previously explored multi-compartment models.

In the current study, we have measured voxelwise longitudinal developmental changes in isotropic and anisotropic restricted (intracellular) diffusion across a large sample size (n=8,039) of youth in late childhood. This unprecedented sample and small age range at each time point (9-11 years at baseline; 11-13 years at follow-up) provides high power to delineate developmental microstructural changes across the WM and increased precision for estimating the magnitude of these effects.

# METHODS

## Sample

The ABCD study is a longitudinal study across 21 data acquisition sites following 11,880 children starting at 9-11 years. This paper uses baseline and two-year follow up (FU) data from the NIMH Data Archive ABCD Collection Release 3.0 (DOI: 10.15154/1519007). The ABCD cohort is epidemiologically informed (Garavan et al., 2018), therefore includes participants from demographically diverse backgrounds, and has an embedded twin cohort and many siblings. Exclusion criteria for participation in the ABCD Study were limited to: 1) lack of English proficiency; 2) the presence of severe sensory, neurological, medical or intellectual limitations that would inhibit the child's ability to comply with the protocol; 3) an inability to complete an MRI scan at baseline. The study protocols are approved by the University of California, San Diego Institutional Review Board. Parent/caregiver permission and child assent were obtained for each participant.

All statistical analyses included 12,525 observations with 8,039 unique subjects, such that 4,486 subjects had data at two time points. Observations were included in the final sample if the participant had complete data across sociodemographic factors (household income, highest parental education, ethnicity), available genetic data (to provide ancestry information using the top 10 principal components), available imaging data that passed all diffusion inclusion criteria and available information regarding acquisition scanner ID and software version. In the ABCD Study, Release 3.0, there are 16727 available scans with scanner information (9.3% missingness). Of these scans, 1728 were excluded for not meeting the recommended dMRI inclusion criteria outlined in the Release 3.0 release notes (tabulated variable: imgincl_dmri_include = 0) and an additional 20 observations were excluded for poor registration defined below (in *Atlas Registration*). The final sample included all remaining observations that had complete data for the previously listed information. Table 1 shows the demographics of the final sample used for statistical analysis stratified by event. Participants who had competed their 2 year follow up in Release 3.0 were more likely to have higher household income, higher parental education and have male assigned as their sex at birth. This may reflect differences in recruitment procedures over the course of recruitment in order to ensure the final sample reflected the demographics of the US population as closely as possible.

| | ***Baseline*** | ***2 Year FU*** | ***p*** |
|---|---|---|---|
| ***n*** | **8039** | **4486** | |
| ***interview_age, mean (SD)*** | 119.23 (7.51) | 143.08 (7.63) | <0.001 |
| ***sex = M, n (%)*** | 4162 (51.8) | 2419 (53.9) | 0.022 |
| ***household.income, n (%)*** | | | <0.0001 |
| *[<50K]* | 2203 (27.4) | 1050 (23.4) | |
| *[>=50K & <100K]* | 2303 (28.6) | 1280 (28.5) | |
| *[>=100K]* | 3533 (43.9) | 2156 (48.1) | |
| ***high.educ, n (%)*** | | | 0.956 |
| *< HS Diploma* | 293 ( 3.6) | 159 ( 3.5) | |
| *HS Diploma/GED* | 594 ( 7.4) | 334 ( 7.4) | |
| *Some College* | 2008 (25.0) | 1096 (24.4) | |
| *Bachelor* | 2183 (27.2) | 1221 (27.2) | |
| *Post Graduate Degree* | 2961 (36.8) | 1676 (37.4) | |
| ***race.4level, n (%)*** | | | 0.282 |
| *White* | 5453 (68.5) | 3120 (70.1) | |
| *Black* | 1033 (13.0) | 536 (12.1) | |
| *Asian* | 173 ( 2.2) | 91 ( 2.0) | |
| *Other/Mixed* | 1299 (16.3) | 701 (15.8) | |
| ***ethnicity, n (%)*** | | | 0.521 |
| *hisp = Yes (%)* | 1568 (19.5) | 853 (19.0) | |

***Table 1. Demographics of the sample.*** *Demographic data is shown for age (mean, (SD)), sex at birth, household income, parental education, self-declared race and endorsement of Hispanic ethnicity (n, (%)). These factors are stratified by time point: baseline and 2-year FU. There were significant differences in the socioeconomic status (income and parental education) and sex at birth for those who had 2-year follow up data in Release 3.0 indicative of differences in the demographics of participants as they were recruited. Participants recruited earlier in the study were more likely to have higher household income and parental education and be born male. All of these variables are controlled for in all statistical analyses to account for this.*

## MRI acquisition

The ABCD MRI data were collected across 21 research sites using Siemens Prisma, GE 750 and Philips 3T scanners. Scanning protocols were harmonized across sites. Full details of structural and diffusion imaging acquisition protocols used in the ABCD study have been described previously (Casey et al., 2018; Hagler et al., 2019) so only a short overview is given here. dMRI data were acquired in the axial plane at 1.7mm isotropic resolution with multiband acceleration factor 3. Diffusion-weighted images were collected with seven b=0 s/mm$^2$ frames and 96 non-collinear gradient directions, with 6 directions at b=500 s/mm$^2$, 15 directions at b=1000 s/mm$^2$, 15 directions at b=2000 s/mm$^2$, and 60 directions at b=3000 s/mm$^2$. T1-weighted images were acquired using a 3D magnetization-prepared rapid acquisition gradient echo (MPRAGE) scan with 1mm isotropic resolution and no multiband acceleration. 3D T2-weighted fast spin echo with variable flip angle scans were acquired at 1mm isotropic resolution with no multiband acceleration.

## Image Processing

The processing steps for diffusion and structural MR data are outlined in detail in Hagler et al., (2019). Briefly, dMRI data were corrected for eddy current distortion using a diffusion gradient model-based approach (Zhuang et al., 2006). To correct images for head motion, we rigid-body-registered each frame to the corresponding volume synthesized from a robust tensor fit, accounting for image contrast variation between frames. Dark slices caused by abrupt head motion were replaced with values synthesized from the robust tensor fit, and the diffusion gradient matrix was adjusted for head rotation (Hagler et al., 2009, 2019). Spatial and intensity distortions caused by B0 field inhomogeneity were corrected using FSL's *topup* (Andersson et al., 2003) and gradient nonlinearity distortions were corrected for each frame (Jovicich et al., 2006). The dMRI data were registered to T1w structural images using mutual information (Wells et al., 1996) after coarse pre-alignment via within-modality registration to atlas brains. dMRI data were then resampled to 1.7 mm isotropic resolution, equal to the dMRI acquisition resolution.

T1w and T2w structural images were corrected for gradient nonlinearity distortions using scanner-specific, nonlinear transformations provided by MRI scanner manufacturers (Jovicich et al., 2006; Wald et al., 2001) and T2w images are registered to T1w images using mutual information (Wells et al., 1996). Intensity inhomogeneity correction was performed by applying smoothly varying, estimated B1-bias field (Hagler et al., 2019). Images were rigidly registered and resampled into alignment with a pre-existing, in-house, averaged, reference brain with 1.0 mm isotropic resolution (Hagler et al., 2019).

## Microstructural models

*Restriction spectrum imaging (RSI)*

The RSI model was fit to the diffusion data to model the diffusion properties of the cerebral tissue (White et al., 2013, 2014). RSI estimates the relative fraction that separable pools of water within a tissue contribute to the diffusion signal, based on their intrinsic diffusion characteristics. Free water (e.g., CSF) is defined by unimpeded water diffusion. Hindered diffusion follows a Gaussian displacement pattern characterised by the presence of neurites (axons and dendrites), glia and other cells. This includes water both within the extracellular matrix and certain intracellular spaces with dimensions larger than the diffusion length scale (typically, ~10μm, with the diffusion sequences used in human imaging studies (White et al., 2013)). Restricted diffusion follows a non-Gaussian pattern of displacement and describes water within intracellular spaces confined by cell membranes. Imaging scan parameters determine the sensitivity of the diffusion signal to diffusion within these separable pools. At intermediate b-values (b=500-2500s/mm$^2$), the signal is sensitive to both hindered and restricted diffusion; whereas, at high b-values (b=3000s/mm$^2$), the signal is primarily sensitive to restricted diffusion. The hindered and restricted compartments are modeled as fourth order spherical harmonic (SH) functions and the free water compartment is modelled using zeroth order SH functions. The longitudinal diffusivity (LD) is held constant, with a value of $1 \times 10^{-3}$ mm$^2$/s for the restricted and hindered compartments. For the restricted compartment, the transverse diffusivity (TD) is fixed to 0

$mm^2/s$. For the hindered compartment, TD is fixed to $0.9 \times 10^{-3}$ $mm^2/s$. For the free water compartment the isotropic diffusivity is fixed to $3 \times 10^{-3}$ $mm^2/s$. Theoretically, any increases in the tortuosity of the hindered compartment, for example due to a decrease in the volume of the extracellular space, will decrease the effective diffusivity in the hindered compartment; however, in our model we are assuming the hindered diffusivity is constant. Spherical deconvolution (SD) is used to reconstruct the fiber orientation distribution (FOD) in each voxel from the restricted compartment. The restricted anisotropic measure, ND, is the norm of the SH coefficients for the second and fourth order SHs (divided by the norm of all the coefficients across the restricted, hindered and free water compartments). This models oriented diffusion emanating from multiple directions within a voxel. The restricted isotropic measure, N0, refers to the spherical mean of the FOD across all orientations (zeroth order SH divided by the norm of all the coefficients across the restricted, hindered and free water compartments).

In this study we explore associations between age and the rotation-invariant features of the restricted compartment FOD. For a detailed description of the derivation of the RSI model see White et al. (2013). We extracted a measure of the restricted isotropic and restricted directional diffusion signal. Within each voxel the total diffusion signal, S, can be represented as

$$S = \sum \beta_{flm} Y_{flm}$$

where $Y_{flm}$ is a SH basis function of order $l$ and degree $m$ of the FOD corresponding to the $f$th compartment, and $\beta_{flm}$ are the corresponding SH coefficients. The measure of restricted isotropic diffusion is given by the coefficient of the zeroth order SH coefficient, $\beta_{f,l=0,m=0}$, normalized by the Euclidian norm of all $\beta_{flm}$ and termed N0:

$$N0 = \frac{|\beta_{f,l=0,m=0}|}{||\beta_{flm}||^2}$$

The measure of restricted normalized anisotropic diffusion is given by the norm of $\beta_{flm}$, where $l > 0$ and $f$ is the restricted compartment, and is termed ND:

$$ND = \frac{|\beta_{f,l>0,m}|}{||\beta_{flm}||^2}$$

These normalized RSI measures are unitless and range from 0 to 1. As N0 and ND are normalized with respect to the hindered and free water compartments, changes in restricted diffusion will be relative to the other compartments. The relative size and shape of restricted compartments will differentially modulate isotropic and anisotropic diffusion.

The magnitude of diffusion that we are sensitive to is dependent on the diffusion scan parameters. Typical diffusion times used in clinical DWI scans are approximately 10–50ms corresponding to average molecular displacements on the order of 10μm (Mukherjee et al., 2008). Any water displacements smaller than this scale would not lead to changes in the measured diffusion coefficient, but changes in cell size <~10μm could alter the relative signal fractions of hindered and restricted diffusion in a voxel. Diffusion estimated in these compartments is also dependent on the permeability of cellular membranes; greater exchange across intracellular and extracellular space will mean that diffusion will appear more hindered rather than restricted.

*Diffusion tensor imaging*

The diffusion tensor model (Basser et al., 1994; Basser & Pierpaoli, 1996) was used to calculate fractional anisotropy (FA) and mean diffusivity (MD). Diffusion tensor parameters were calculated using a standard, linear estimation approach with log-transformed diffusion-weighted (DW) signals (Basser et al., 1994). Tensor matrices were diagonalized using singular value decomposition, obtaining three eigenvectors and three corresponding eigenvalues. FA and MD were calculated from the eigenvalues (Basser & Pierpaoli, 1996).

## Atlas registration

To allow for voxelwise analysis, subjects' imaging data were aligned using a multimodal nonlinear elastic registration algorithm. At the end of the preprocessing steps outlined in *Image Processing* and described in detail in Hagler et al. (2019), subjects' structural images and diffusion parameter maps were aligned to an ABCD-specific atlas, using a custom diffeomorphic registration method. The ABCD-specific atlas was constructed using an iterative procedure, consisting of an initial affine registration, followed by a multi-scale, multi-channel elastic diffeomorphic registration. Imaging volumes used for the elastic registration included 3D T1 and direction-encoded color (DEC) FA volumes (x-, y- , and z-orientations). After each iteration, morphed volumes for each subject were averaged to create an updated atlas, and then the process was repeated until convergence. Participants with poor registration to atlas were excluded from the average and subsequent statistical analyses. Poor registration was defined as a voxelwise correlation to atlas <0.8 (see *Sample* for number excluded).

## Labelling regions of interest (ROI)

Subcortical structures were labeled using Freesurfer 5.3 (Fischl et al., 2002). Subjects' native space Freesurfer parcellations were warped to the atlas space and averaged across subjects. Bilateral binary masks for each ROI were created using a probabilistic threshold of 0.8. For each subject, mean WM diffusion measures were generated by averaging N0, ND, FA and MD across all voxels in a WM mask generated from the Freesurfer segmentation (not including cerebellar WM). Major white matter tracts were labelled using AtlasTrack, a probabilistic atlas-based method for automated segmentation of white matter fiber tracts (Hagler et al., 2009, 2019). Unilateral binary masks for each ROI (except the CC, Fmaj and Fmin which are interhemispheric) were created by thresholding at 40% of the maximum relative probability across the ROI. A list of WM tract ROIs used in this study is listed in Supplementary Table 1.

## Statistical analysis

Univariate general linear mixed effects models (GLMMs) were applied at each voxel to test the associations between age and diffusion metrics: N0, ND, FA and MD. Age was divided into two predictors: baseline age ($age_0$) and change in age from baseline to 2 year follow up ($age_\Delta$). A contrast ($age_0$=1, $age_\Delta$=-1) was used to measure significant differences in the voxelwise estimated beta

coefficients for $age_0$ and $age_\Delta$. Interactions between each age predictor and sex were included in the model: $age_0$*sex; $age_\Delta$*sex. Given the demographic diversity in the sample, all statistical analyses controlled for the variables shown in Table 1, except fixed effects of the top 10 genetic principal components were used to account for ancestry effects in lieu of self-declared race. Additional fixed effects included scanner ID and MRI software version. Random effects of family ID and subject ID were also modelled. Whole-brain voxelwise analyses were corrected for multiple comparisons at an alpha level of 0.05 using a Bonferroni correction across 155,179 voxels (threshold for voxelwise significance: $|t|=4.98$, uncorrected $-\log_{10}(p)=6.49$). This provides a conservative estimate of significant developmental effects as the true number of independent tests is likely to be smaller than this. T-statistic maps thresholded to correct for multiple comparisons across the whole brain are presented in the supplementary materials. Unthresholded effect size maps are shown in the main figures to provide a comprehensive description of the distribution of estimated effects across the brain. ROI analyses were also conducted using the same GLMMs by taking the mean diffusion metric across the voxels within each ROI mask as the dependent variable in order to provide an estimate of the developmental effect for each WM tract. Violin plots were generated to show the variability in voxelwise effects across all voxels within each ROI mask in order to highlight the heterogeneity of developmental effects within each WM tract. P-values were adjusted for multiple comparisons at an alpha level of 0.05 based on 27 independent tests (threshold for ROI-wise significance: $|t|=2.89$, uncorrected $-\log_{10}(p)=2.72$, corrected $-\log_{10}(p)=1.3$).

# RESULTS

## Global developmental effects of restricted diffusion across the WM

In order to examine global developmental changes in N0 and ND, we measured age associations with mean N0 and mean ND averaged across voxels within a WM mask (across hemispheres). From herein, these mean measures will be referred to as global N0 and global ND. Both global measures showed significant positive associations with age (N0 $age_0$: $t=19.17$, $-\log_{10}(p)=81$; N0 $age_\Delta$: $t=36.19$, $-\log_{10}(p)=286$; ND $age_0$: $t=14.19$, $-\log_{10}(p)=45$; ND $age_\Delta$: $t=35.59$, $-\log_{10}(p)=277$; Figure 1). Global N0 showed a significantly lower beta coefficient for the $age_\Delta$ association compared to the beta coefficient for the $age_0$ association ($t=3.55$, $-\log_{10}(p)=3.4$). There was no significant difference in the beta coefficients for the $age_\Delta$ and $age_0$ association for global ND. Global FA and global MD (defined in the same way as global N0 and ND) also showed significant associations with $age_0$ and $age_\Delta$ with global FA showing a positive association and global MD showing a negative association (supplementary figure 1). There were no $age_0$ by sex or $age_\Delta$ by sex interactions for global N0 or ND, which suggests that, on average, the developmental changes in microstructure shown in the current study did not differ by sex assigned at birth.

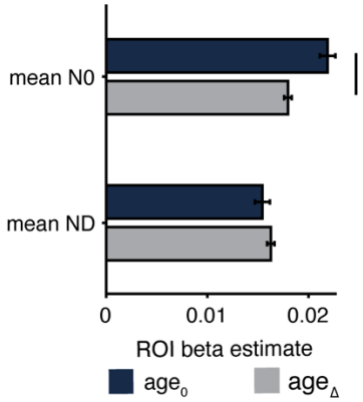


***Figure 1. Age associations global restricted diffusion measures.*** *Mean N0 and mean ND both showed significant positive associations with $age_0$ (blue) and $age_\Delta$ (gray). For mean N0, the estimated $age_\Delta$ association was significantly reduced compared to the $age_0$ association. There was no significant difference between these estimates for mean ND.*

## Regional age associations with restricted isotropic diffusion in WM

Voxelwise associations between age and N0 were positive across the brain, such that greater N0 was associated with older age (Figure 2A,B). The largest voxelwise effects were found in subcortical regions and these are reported on by Palmer et al, (2021). Here we will focus on developmental effects within the WM. The patterns of association across the brain for $age_0$ and $age_\Delta$ were very similar, but the t-statistics were much greater for $age_\Delta$ due to the increased statistical power when estimating longitudinal effects (supplementary figure 2). ROI analyses were conducted to estimate developmental effects across the major WM tracts. We found significant positive developmental effects across all of the WM tract ROIs measured, mirroring our voxelwise analysis (Figure 2C) with the largest association in the left superior corticostriatal tract (SCS) and the smallest association in the forceps minor (Fmin). Supplementary Table 2 shows the statistical output for all of the WM tract ROI analyses. Despite significant ROI associations, there was variability in the $age_\Delta$ association across voxels within each ROI mask, such that not all voxels showed a significant $age_\Delta$ association (figure 2D).

Despite there being a significant difference in the beta coefficient for the $age_0$ and $age_\Delta$ associations with global N0, there were no voxels showing a significant difference between the beta coefficients for $age_0$ and $age_\Delta$ after correction for multiple comparisons. This is likely due to the stringent control for multiple comparisons in our voxelwise analysis. In contrast, for nearly all of the WM tract ROIs, the beta coefficient for the ROI $age_\Delta$ association was significantly smaller than for $age_0$, similar to the global N0 effect. These effect sizes were small in comparison to the main effects of age, which in part explains why the voxelwise differences did not survive correction for multiple comparisons (supplementary table 2).

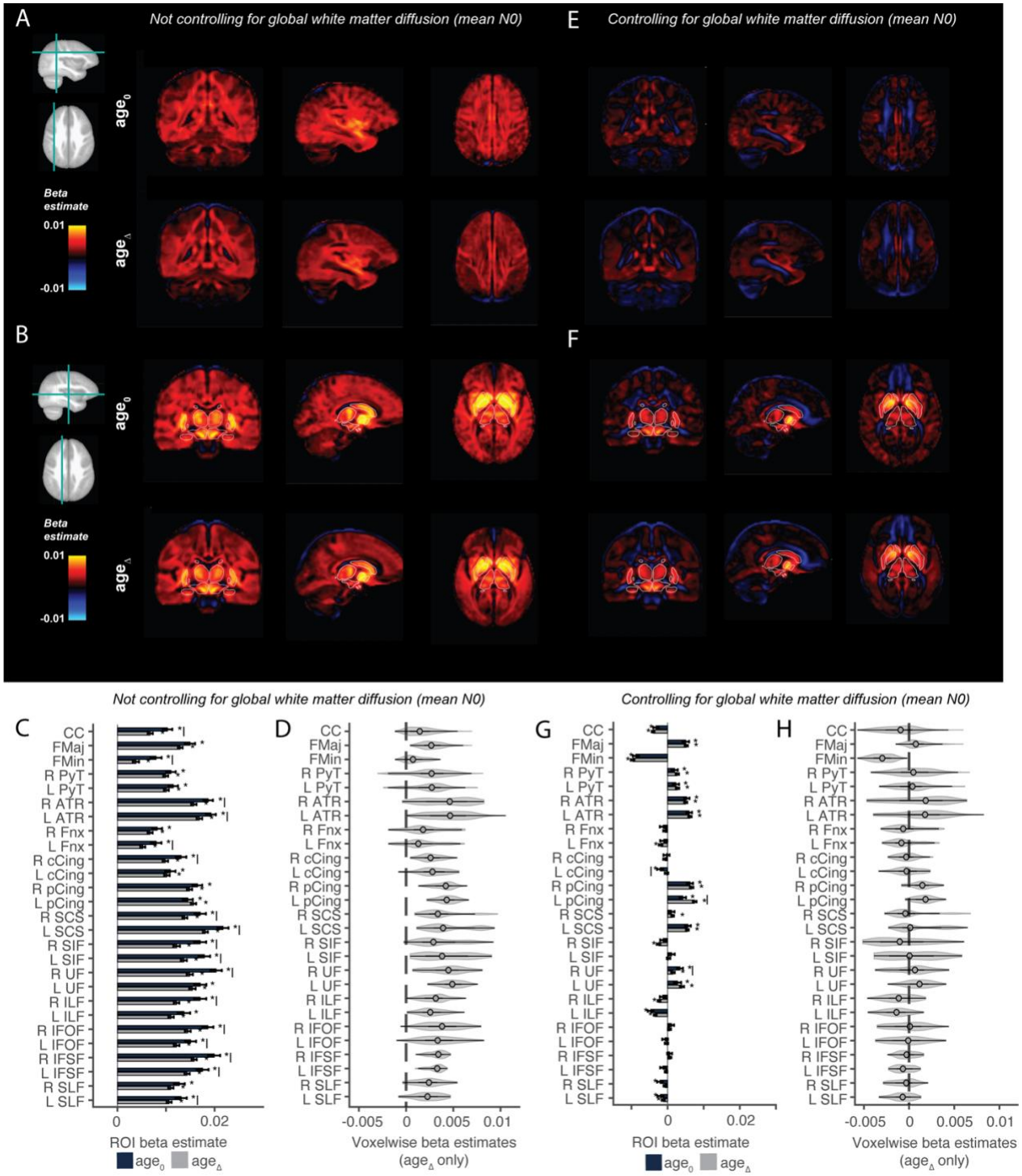


***Figure 2. Associations between age$_0$ and age$_\Delta$ and restricted isotropic diffusion, N0.*** *A,B) Voxelwise beta coefficients for the association between N0 and age$_0$ and age$_\Delta$ across different brain slices not controlling for global N0. Outlines of the subcortical FreeSurfer ROIs are overlaid for the thalamus, caudate, pallidum, putamen, ventral diencephalon, amygdala and hippocampus to orient the reader. C) ROI analyses of the associations between N0 and age$_0$ (dark blue) and age$_\Delta$ (gray) without controlling for global N0. D) Violin plots showing the distribution of voxelwise age$_\Delta$ associations in each ROI without controlling for global N0. E-H) Same plots as A-D but with a model controlling for global N0. Asterisks denote significant associations (corrected p-value threshold of -log$_{10}$(p)=2.72). Solid lines represent significant difference between age$_0$ and age$_\Delta$ coefficients. WM tract ROI abbreviations described in Supplementary Table 1.*

In order to determine if there was any regionalization of developmental associations, i.e., regions that had a greater or smaller age effect relative to the global (mean) effect, we conducted additional analyses controlling for global N0. The voxelwise $age_0$ and $age_\Delta$ associations were substantially reduced across the WM, such that many voxels were no longer significant (Figure 2E,F). Voxels showing statistically significant associations after correction for multiple comparisons across the brain are shown in Supplementary Figure 2. Relative to the global effect, there was a posterior-anterior gradient of developmental effects. There were voxels within the anterior WM, such as the Fmin and frontal/superior portions of the body of the corpus callosum (CC), anterior thalamic radiations (ATR), striatal inferior frontal cortical tracts (SIF) and the SCS, that showed a significant negative association when controlling for global N0 indicating a reduced developmental effect relative to the global effect; whereas, voxels within the posterior WM showed a significant positive age association when controlling for the global N0 indicating a greater developmental effect relative to the global effect. The exception to this pattern was the inferior longitudinal fasciculus (ILF), the fornix (Fnx), and the posterior (occipital) portion of the inferior frontal occipital fasciculus (IFOF), where voxels showed a reduced developmental effect relative to the global effect. Voxels in and surrounding the subcortical structures remained significantly positively associated with age when controlling for global N0. This suggests that individual variability in the development of N0 in subcortical regions is orthogonal to the individual variability in the development of global N0 across the WM (superior to the subcortical space).

When controlling for global N0 in the ROI analyses, significant positive associations remained for the forceps major (FMaj), bilateral pyramidal tract (PyT), ATR, parahippocampal cingulum (pCing), uncinate fasciculus (UF), and the left SCS (Figure 2G). Significant negative associations when controlling for global N0 were found in the CC, Fmin, left Fnx, right SIF, and bilateral ILF. Developmental effects varied within these fiber tracts, highlighting heterogeneity in the distribution of $age_\Delta$ associations within these ROIs (Figure 2H). In particular, positive associations relative to global N0 appeared to be driven by voxels near or overlapping with subcortical regions. This can clearly be seen for the SCS, where voxels in anterior inferior portions of the tract overlapping with the putamen ROI showed significant positive associations, but voxels superior to the putamen within the SCS did not (Figure 4A). For the PyT, the significant ROI association appeared to be driven by voxels in the PyT overlapping with the ventral diencephalon (Figure 4B). Similarly, along the ATR, age associations were greater relative to the global effect in voxels overlaying with the thalamus and reduced relative to the global effect in anterior voxels close to Fmin (Figure 4C). Developmental associations did not only occur within voxels with the highest mean N0 across subjects, which suggests these effects were not necessarily driven by the size of the restricted signal fraction in each voxel.

## Regional age associations with restricted anisotropic diffusion in WM

Voxelwise associations between $age_0$, $age_\Delta$ and ND revealed a developmental increase in ND across the brain with age (Figure 3A,B). Unlike N0, developmental effects were greatest along the center of WM tracts where anisotropy was highest. Age associations with ND were smaller than those with N0. Voxels showing statistically significant associations, after correction for multiple comparisons, are

shown in Supplementary Figure 2. ROI analyses demonstrated significant positive age associations across all of the WM tracts (Figure 3C). Supplementary Table 2 shows the statistical output for all of the WM tract ROI analyses. Despite significant mean associations within each ROI, there was substantial variability in the $age_{\Delta}$ associations across voxels within each ROI mask (figure 3D). Unlike for N0, for both the voxelwise and ROI ND analyses, there was no evidence that the $age_{\Delta}$ developmental effects were significantly lower than the $age_0$ effects, suggesting the development of ND in the WM is likely to be linear from 9-13 years. The pCing was the only ROI to show a significant difference in these coefficients, and here the $age_{\Delta}$ association was larger than the $age_0$ association.

To determine whether the individual variability in the developmental effect for any WM region was independent from the global effect, we conducted additional analyses including global ND as a covariate. This resulted in a large decrease in the association between ND and $age_0$, and $age_{\Delta}$ across the WM such that the majority of voxels no longer showed a significant association, particularly for the $age_0$ associations, which have less statistical power (Figure 3E,F,H). Statistically significant associations, after multiple comparisons correction, are shown in Supplementary Figure 2. Similar to N0, the pattern of effect sizes across the brain suggests a posterior-anterior gradient of development. There were voxels in frontal WM that showed significant negative age associations when controlling for global ND, indicating reduced developmental effects in these regions relative to the global effect. There were, in contrast, positive associations in posterior WM, however, unlike for N0, many voxels did not reach our conservative corrected threshold for significance.

Developmental effects estimated within each ROI controlling for global ND were also substantially attenuated (Figure 3G). Significant positive associations remained for the FMaj, bilateral PyT, ATR, pCing, SCS and ILF, and left UF. ND in the ILF had a greater age association relative to the global ND effect, in contrast to N0 in this tract, where there was a smaller association between N0 and age relative to the global N0 effect. Significant negative associations when controlling for global ND were found in the CC, Fmin, right Fnx, right UF, bilateral SIF, IFOF and SLF.

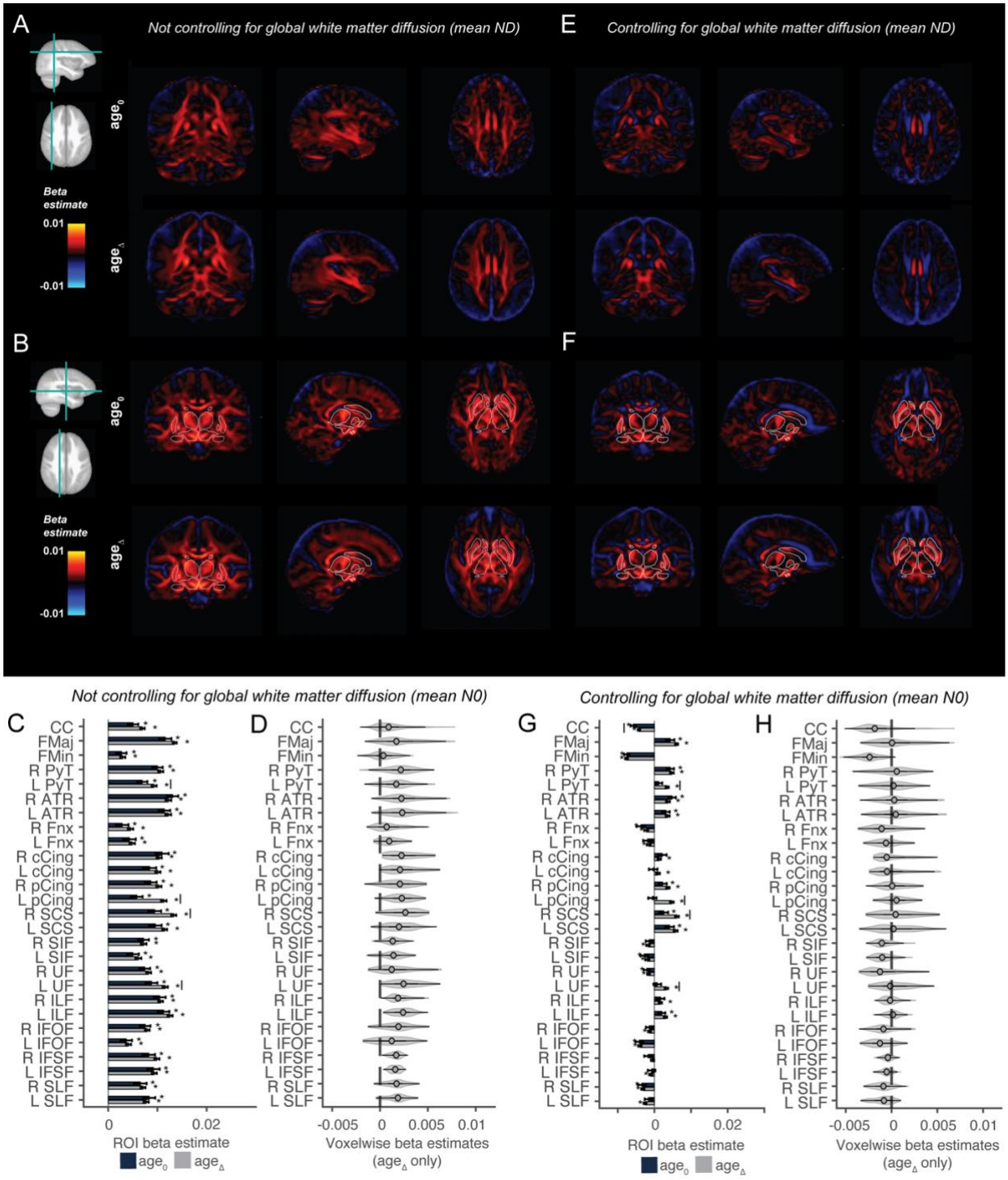


***Figure 3. Associations between $age_0$ and $age_\Delta$ and restricted anisotropic diffusion, ND.*** *A,B) Voxelwise beta coefficients for the association between ND and $age_0$ and $age_\Delta$ across different brain slices not controlling for global ND. Outlines of the subcortical Freesurfer ROIs are overlaid for the thalamus, caudate, pallidum, putamen, ventral diencephalon, amygdala and hippocampus to orient the reader. C) ROI analyses of the associations between ND and $age_0$ (dark blue) and $age_\Delta$ (gray) without controlling for global ND. D) Violin plots showing the distribution of voxelwise $age_\Delta$ associations in each ROI without controlling for global ND. E-H) Same plots as A-D but with a model controlling for global ND. Asterisks denote significant associations (corrected p-value threshold of $-\log_{10}(p)=2.72$). Solid lines represent significant difference between $age_0$ and $age_\Delta$ coefficients. WM tract ROI abbreviations described in Supplementary Table 1.*

Voxelwise associations showed less heterogeneity within WM ROIs for ND compared to N0, however, similar to N0, associations in fiber tract voxels adjacent to or overlapping with subcortical ROIs, such as the PyT, ATR and SCS, showed high heterogeneity, particularly when controlling for mean ND. Voxels in the SCS overlapping with the putamen ROI (Figure 4A), voxels within the PyT superior to the ventral diencephalon (Figure 4B) and voxels within the ATR overlapping with the thalamus ROI (Figure 4C) showed greater age associations relative to the global effect, whereas superior and anterior voxels within these tracts closer to the cortex showed reduced age associations that were in many voxels not significant. This demonstrates that individual variability in the development of ND in these more inferior WM tract voxels close to and overlapping with subcortical regions is independent of, and changing more quickly than, the development of global ND. For the SCS in particular, the voxels that showed significant positive age associations after controlling for global ND showed the primary orientation of the FODs in the anterior-posterior (green) direction, whereas more superior voxels showed diffusion primarily oriented in the superior-inferior (blue) direction as expected for diffusion along the SCS (Figure 4). This suggests that the developmental ROI effect in the SCS after controlling for global ND was likely driven by orthogonal developmental changes in restricted diffusion in voxels where the SCS innervates the putamen. In addition, the FMaj and the cingulate cingulum (cCing) showed high heterogeneity driven by larger positive associations around the edge of the ROI boundary, which may be due to partial voluming effects of the ventricles for the FMaj and the underlying cortex for the cCing.

## Developmental effects of restricted diffusion along the gray-white matter boundary

For both N0 and ND, after controlling for the respective global WM measure, there were voxels showing significant $age_0$ and $age_\Delta$ associations located outside of the WM tract ROIs along the gray-white matter boundary. For example, voxels running parallel to the ILF along the boundary of the long posterior gyrus of the insula (Figure 5A), voxels running parallel to the UF along the boundary of the anterior insula (Figure 5B) and voxels running parallel to the cingulum along the boundary of callosal sulcus (Figure 5C). At each of these locations there was a change in the primary FOD direction and a higher likelihood of crossing fibers as seen in the mean FOD images (Figure 5).

## Developmental associations with DTI vs RSI metrics

Supplementary figures 4-6 show the $age_0$ and $age_\Delta$ associations with mean diffusivity (MD) and fractional anisotropy (FA) from the diffusion tensor model. In general, there was a large correspondence between the MD and N0 developmental associations (in opposite directions) across the WM. There were differences, however, between the FA and ND associations. Namely, the magnitude of the FA associations across the brain was much smaller than that of ND, such that a larger sample would be required to detect developmental FA associations compared to ND. However, the pattern of associations across the brain was similar.

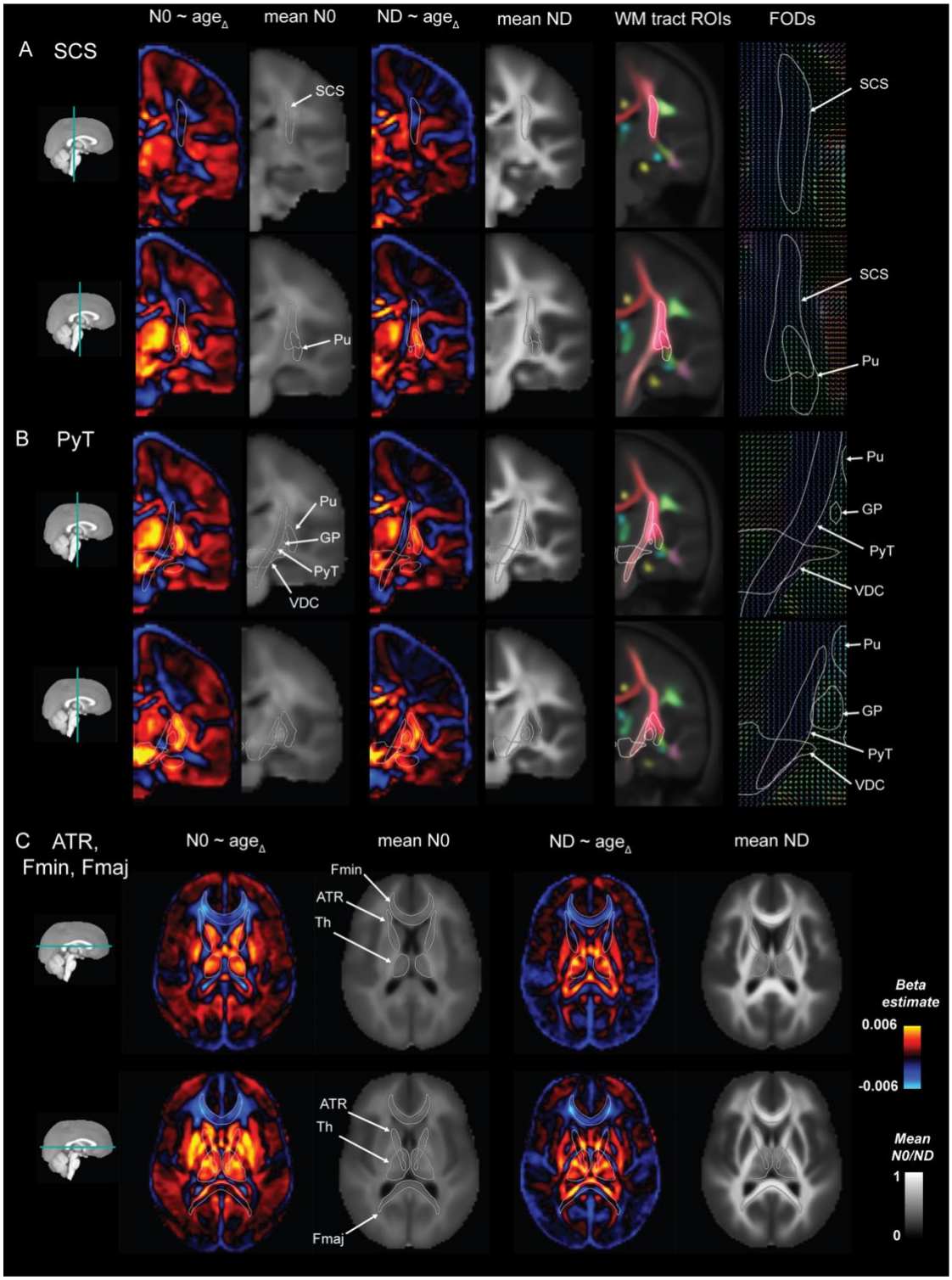


***Figure 4. Associations between age$_\Delta$ and N0 and ND with respect to specific tracts, controlling for global N0 and global ND, respectively.*** *Unthresholded age$_\Delta$ beta estimates shown for the SCS (A), PyT (B) and ATR (C) for N0 (column 1) and ND (column 3) alongside voxelwise mean N0 (column 2) and voxelwise mean ND (column 4). Panels A&B show voxelwise ROIs of WM tracts identified using AtlasTrack (column 5): SCS (dark pink) and PyT (light pink); and a close-up of the voxelwise cohort-averaged FODs in that region (column 6). A) The SCS fiber tract outline is shown alongside the outline of the putamen (Pu) in two slices moving from posterior (top image) to anterior (bottom image). Positive associations after controlling for global N0 and global ND remain significant in voxels overlapping with the Pu where the primary orientation of diffusion changes from superior-inferior (blue) in superior voxels of the SCS to anterior-posterior (green) in the region of the Pu. B) PyT fiber tract outline is shown running alongside the Pu (top image; posterior) and globus pallidus (GP; bottom image; anterior) and through the ventral diencephalon (VDC). Anterior voxels showing positive associations*

*with N0 in the PyT (after controlling for global N0) are located within the VDC (B, column 1, bottom) and positive associations for ND were located superior to the VDC to the GP. C) Anterior portions of the ATR adjacent to the Fmin (C, top) showed negative N0 developmental associations (after controlling for global N0), whereas posterior inferior portions of the ATR (C, bottom) showed positive associations in voxels adjacent to and overlapping with the thalamus (Th) for N0 and ND. WM tract ROI abbreviations described in Supplementary Table 1.*

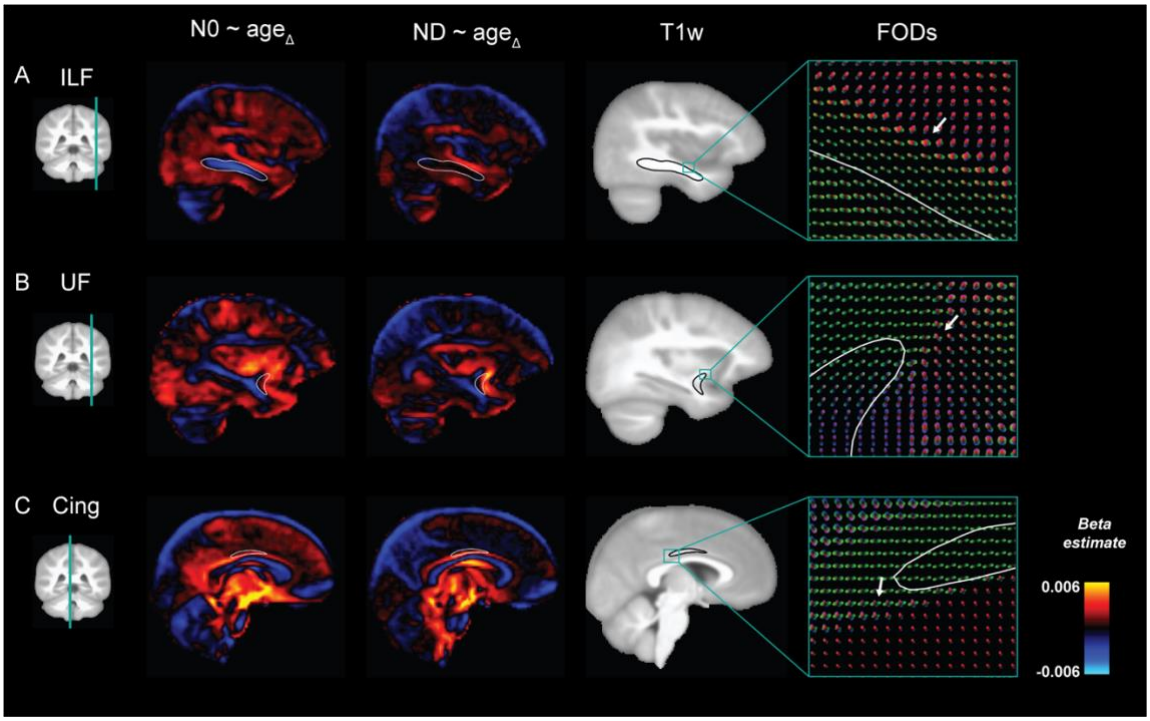


***Figure 5. Associations between age$_\Delta$ and N0 and ND in voxels along the gray-white matter boundary.*** *Unthresholded beta coefficients for the age$_\Delta$ associations shown for N0 controlling for mean N0 (column 1) and ND controlling for mean ND (column 2). The T1w image for the same slices is shown (column 3) and a close-up of the cohort-averaged FODs (column 4) in that region. A) Age$_\Delta$ associations run parallel to the ILF (outlined) along the long posterior gyrus of the insula for N0 and ND. B) Age$_\Delta$ associations run parallel to the UF (outlined) along the edge of the anterior insula with short-connections to the orbitofrontal cortex for N0 and ND. C) Age$_\Delta$ associations run parallel to the cingulum along the callosal sulcus for N0 and ND. WM tract ROI abbreviations described in Supplementary Table 1. White arrows indicate FODs showing anisotropic diffusion in multiple orientations.*

# DISCUSSION

In the current study, we have shown significant increases in restricted (intracellular) diffusion across the WM in a large sample of children from 9 to 13 years of age (n=8,039). This is the largest study to date measuring longitudinal changes in diffusion metrics in WM at this age. There was a significant increase in global (mean) N0 and ND across the WM. For global N0, the longitudinal age effect was significantly smaller than the cross-sectional effect, which suggests that N0 in the WM may follow a non-linear trajectory from 9-13 years. However, this was not the case for ND, which likely follows a linear trajectory in this age range. Controlling for variability in global RSI measures led to a large attenuation of voxelwise age associations across the WM, indicative of a global developmental effect. There was limited regionalization of effects across WM tracts; however, there were some regions across the brain where variability in the development of restricted diffusion was independent of this

global effect. Firstly, voxels within WM tracts overlapping with or adjacent to subcortical ROIs showed positive development effects independent of the global effect. Secondly, voxels within frontal WM showed reduced development of restricted diffusion relative to the global effect. Finally, voxels along gray-white matter boundaries parallel to the Cing, UF and ILF showed independent developmental effects relative to the global effect. These findings highlight the benefit of voxelwise compared to ROI-wise analyses for understanding the pattern of development across the brain. Future work will aim to determine whether individual variability in the maturation of tissue microstructure in particular regions relates to cognitive and behavioral development.

There was a robust global increase in restricted diffusion from 9-13 years across the WM. By controlling for global RSI measures, we were able to test for regionalization across the WM. The relative differences in development across WM tracts is not currently well-defined in the literature due to small sample sizes across different age ranges and differences in the models used to map developmental trajectories. In our analyses, age associations across the WM were significantly attenuated when controlling for the respective global measures with limited evidence for regionalization. The remaining significant positive ROI associations for both N0 and ND (ATR, PyT, pCing and SCS) appeared to be driven by voxels within or near subcortical structures. For the SCS, the tractography used to generate the SCS tract ROI included termination points in the striatum (Hagler et al., 2019), therefore the overlap of the SCS ROI and the putamen ROI is likely indicating voxels in which the SCS is innervating the putamen. The positive associations in this region when controlling for the global RSI measures suggests that individual variability in the development of restricted diffusion at this innervation point contains variability orthogonal to the development of the rest of the WM. The same could be seen for the ATR; in the original tractography all streamlines for the ATR were set to terminate on one end of the thalamus and not pass out the back of the thalamus. The independent development of restricted diffusion across these subcortical regions may be specific to the refinement of particular circuits important in reward and affective processing. This is discussed in more detail in Palmer et al (2021). Moreover, there were tracts that showed significantly smaller developmental effects relative to the global effect, namely in the Fmin, CC (of which Fmin is a subset) and Fnx for N0 and ND, the ILF for N0 only, and the IFOF and SLF for ND only. Subsequent longitudinal data across more than two time points is required to estimate non-linear developmental trajectories of restricted diffusion in these tracts in order to determine if there are further distinctions in regional development as alluded to in the literature (Lebel et al, 2008; Chang et al, 2015). These analyses highlight the importance of measuring voxelwise associations to avoid the misleading impression of homogeneity of effects across the entirety of WM tracts. This has been eloquently shown using a similar model of intracellular diffusion (Lynch et al., 2020).

In the corpus callosum (CC), N0 and ND both increased with age, however, the magnitude of the age associations differed along the posterior-anterior axis. This was particularly clear when controlling for the global WM effect. Voxels in the Fmaj, which connects the two occipital lobes at the back of the brain and is the occipital portion of the CC, showed a greater developmental effect than voxels in the

Fmin, which connects the lateral and medial surfaces of the frontal lobes and is the frontal portion of the CC,. Our results support previous evidence from other developmental samples showing a greater age effect of intracellular diffusion metrics in the splenium or forceps major compared to the genu or forceps minor (Geeraert et al., 2019; Genc, Seal, et al., 2017; Mah et al., 2017) and the more extended development of frontal-temporal connections (Genc, Seal, et al., 2017; C. Lebel et al., 2008; Catherine Lebel & Beaulieu, 2011b; Tamnes et al., 2010). This mirrors the posterior-anterior sequence of myelination in developing infants (Bird et al., 1989; Kinney et al., 1988), suggesting differences in the time-course of myelination across the CC may be contributing to the effects here. In addition, Genc et al found that from 4-19 years, age showed a greater positive association with apparent fiber density (a measure of the intracellular volume fraction) in posterior relative to anterior portions of the CC (Genc et al., 2018). This suggests that changes in axonal diameter and/or myelination, that can contribute to increases in the restricted volume fraction, likely occur at a different rate depending on the location in the CC. Different sections of the CC connect different cortical regions within distinct functional networks. Nonuniformity in the development of these interhemispheric connections may reflect age-dependent maturation of cognitive and behavioral processes. More protracted developmental changes in frontal circuitry may underpin the later development of cognitive control in adolescence and become more prominent as the children get older (Casey et al., 2008).

Additionally, we found significant age effects for N0 and ND running parallel to WM tracts along the gray-white matter boundary within particular regions, namely inferior to the cingulum along the edge of the callosal sulcus, lateral to the UF along the boundary of the anterior insula where short range connections connect to orbitofrontal cortex (Catani et al., 2012) and anterior to the ILF along the boundary of the posterior long gyrus of the insula (Uddin et al., 2017). These voxels remained positively associated with age after controlling for the global mean WM metric highlighting that there is residual, unique variability in age-related microstructural changes in these regions orthogonal to and greater than the mean WM effect. These developmental associations are likely driven by increased myelination and/or caliber of cortico-cortical neurons at the gray-white matter boundary, such as short-range U-fibers that connect adjacent cortical regions (Catani et al., 2012; Ouyang et al., 2017; Tusa & Ungerleider, 1985). Indeed, gray-white matter contrast has been shown to be a good predictor of age and this likely contributes in part to developmental decreases in apparent cortical thickness (Jernigan et al., 2011; Lewis et al., 2018). Deviations in the maturation of gray-white contrast across the brain have been associated with cognitive function in typically developing children and autism spectrum disorder (Bezgin et al., 2018; Lewis et al., 2018); therefore, individual variability in microstructural development along these boundaries may be important for understanding individual variability across different cognitive tasks. Indeed, the insular cortex in particular has several functional roles in sensorimotor integration, attention and salience processing and socio-emotional function that are all developing in this age range (Menon & Uddin, 2010; Uddin et al., 2017).

In general, N0 showed more widespread effects across the WM compared to ND, which showed larger developmental effects along the centers of WM tracts where axonal coherence is highest. Differential

patterns in the magnitude of developmental effects for N0 and ND across the brain demonstrate the relative increase in isotropic compared to anisotropic restricted diffusion with age across different regions. There are several biological processes that may increase restricted diffusion in the WM, such as increasing myelination, neurite density and/or axon coherence (described in more detail in Palmer et al, 2021). Previous studies using NODDI have shown age-related changes in NDI (a measure of the intracellular volume fraction) in a similar age range in the WM, and no changes in the orientation dispersion index (ODI; a measure of the degree of dispersion of neurites). This suggests axon geometry may remain constant across this age range (Chang et al., 2015; Genc, Seal, et al., 2017; Mah et al., 2017). Increases in NDI have been associated with increases in the myelin volume fraction using MRI (Geeraert et al., 2019) and post-mortem histology from patients with demyelination (Grussu et al., 2017). In general, there has been a lack of evidence for increasing myelination in late childhood as measured with magnetization transfer (Geeraert et al., 2019; Moura et al., 2016; Pangelinan et al., 2016). However, given histological findings that myelination continues into adulthood (Benes, 1989; Yakovlev & Lecours, 1967), these myelin changes may be very subtle, and require large sample sizes and/or longitudinal studies, such as this, to detect. Little is known about how changes in myelination directly impact RSI measures specifically; however, in a demyelinated genetic mouse model, regions with reduced myelin showed reduced intraneurite volume fraction, estimated using a similar spherical deconvolution method (Kaden et al., 2016). Increasing myelination reduces the permeability of myelinated axons and decreases the volume of the extracellular space in a voxel increasing the restricted signal fraction. Therefore, increased myelination with development may underlie the developmental effects recorded here. However, this is one of many biological processes that can alter restricted diffusion, therefore further work is needed to delineate the exact neurobiological processes contributing to the developmental effects reported here.

In the current study, developmental changes in N0 were very similar (but opposite in sign) to those observed in MD, estimated from the diffusion tensor model. As diffusion becomes more restricted, MD within a voxel will decrease. Our analyses showed greater developmental changes in MD compared to FA from 9-13 years, whereas previous studies have shown relatively greater percent changes in FA compared to MD across WM tracts (Krogsrud et al., 2016b; C. Lebel et al., 2008). These studies are difficult to compare directly due to the different age ranges measured and sample sizes. Furthermore, most studies estimate MD using diffusion MRI data acquired at lower b-values (below b=2000 s/mm$^2$) than the current study (which includes many directions at b=3000 s/mm$^2$). At higher b-values, around b=3000s/mm$^2$, the signal from the hindered compartment is attenuated and the measured diffusion signal is dominated by the restricted compartment. If maturational changes are predominantly occurring within the restricted compartment our DTI measures may be more sensitive to age-related changes than DTI metrics from studies with lower b-value acquisitions. Further work empirically comparing developmental effects on MD calculated with different acquisition parameters is required.

In our statistical analyses, we have modelled age using two predictors ($age_0$ and $age_\Delta$). Together these predictors are equivalent to modelling age as a single continuous variable; however, by separating them we can dissociate cross-sectional (between-subject) and longitudinal (within-subject) age associations, thereby providing more information about individual differences in brain development across the cohort. This is particularly useful in the ABCD study as those with two scans in Release 3.0 were all recruited earlier in the study and varied in sociodemographics, particularly household income and highest parental education, compared to the rest of the cohort. In general, the longitudinal age effect for ND was similar to the cross-sectional effect, suggesting a linear trajectory from 9-13 years. However, this was not the case for N0, for which the longitudinal age effect was smaller than the cross-sectional. This may reflect potential cohort differences in brain development between those recruited in the first versus the second half of the study, or could be an indication of a non-linear developmental trajectory in this age range. Subsequent longitudinal data will be required to tease apart these inferences. Given the sociodemographic differences in mean household income and parental education between individuals recruited earlier vs later in the study it will be useful in future analyses with more follow-up time points to measure the interaction between sociodemographic factors and brain development to understand this relationship more fully.

Overall, we have demonstrated global increases in the restricted signal fraction across the WM. Voxels in frontal WM in general showed smaller age-related changes from 9-13 years relative to the global effect and voxels within subcortical regions and along particular gray-white matter boundaries showed greater age-related changes orthogonal to this global effect. These findings may demonstrate important biological maturational processes that will be integral for understanding how particular networks develop in this age range. Interestingly, the orthogonal variability in microstructural development across different brain regions emphasizes a potential novel avenue for understanding differential behavioral profiles across individuals. Understanding whether individual differences in the age-related structural covariance of these measures associates with differential behavioral profiles will provide a promising new avenue for future research.

## FUNDING

Data used in the preparation of this article were obtained from the Adolescent Brain Cognitive Development (ABCD) Study (https://abcdstudy.org), held in the NIMH Data Archive (NDA). This is a multisite, longitudinal study designed to recruit more than 10,000 children age 9-10 and follow them over 10 years into early adulthood. The ABCD Study is supported by the National Institutes of Health and additional federal partners under award numbers U01DA041022, U01DA041028, U01DA041048, U01DA041089, U01DA041106, U01DA041117, U01DA041120, U01DA041134, U01DA041148, U01DA041156, U01DA041174, U24DA041123, U24DA041147, U01DA041093, and U01DA041025. A full list of supporters is available at https://abcdstudy.org/federal-partners.html. A listing of participating sites and a complete listing of the study investigators can be found at https://abcdstudy.org/Consortium_Members.pdf. ABCD consortium investigators designed and implemented the study and/or provided data but did not all necessarily participate in analysis or writing of this report. This manuscript reflects the views of the authors and may not reflect the opinions or views of the NIH or ABCD consortium investigators. The ABCD data repository grows and changes over time. The data was downloaded from the NIMH Data Archive ABCD Collection Release 3.0 (DOI: 10.15154/1519007).

## ACKNOWLEDGEMENTS

The authors wish to thank the youth and families participating in the Adolescent Brain Cognitive Development (ABCD) Study and all ABCD staff involved in data collection and curation. Dr. Dale reports that he was a Founder of and holds equity in CorTechs Labs, Inc., and serves on its Scientific Advisory Board. He is a member of the Scientific Advisory Board of Human Longevity, Inc. He receives funding through research grants from GE Healthcare to UCSD. The terms of these arrangements have been reviewed by and approved by UCSD in accordance with its conflict of interest policies.

# REFERENCES

Andersson, J. L. R., Skare, S., & Ashburner, J. (2003). How to correct susceptibility distortions in spin-echo echo-planar images: Application to diffusion tensor imaging. *NeuroImage*, *20*(2), 870–888. https://doi.org/10.1016/S1053-8119(03)00336-7

Baron Nelson, M., O'Neil, S. H., Wisnowski, J. L., Hart, D., Sawardekar, S., Rauh, V., Perera, F., Andrews, H. F., Hoepner, L. A., Garcia, W., Algermissen, M., Bansal, R., & Peterson, B. S. (2019). Maturation of Brain Microstructure and Metabolism Associates with Increased Capacity for Self-Regulation during the Transition from Childhood to Adolescence. *The Journal of Neuroscience : The Official Journal of the Society for Neuroscience*, *39*(42), 8362–8375. https://doi.org/10.1523/JNEUROSCI.2422-18.2019

Basser, P. J., Mattiello, J., & Lebihan, D. (1994). Estimation of the Effective Self-Diffusion Tensor from the NMR Spin Echo. *Journal of Magnetic Resonance, Series B*, *103*(3), 247–254. https://doi.org/10.1006/jmrb.1994.1037

Basser, P. J., & Pierpaoli, C. (1996). Microstructural and physiological features of tissues elucidated by quantitative-diffusion-tensor MRI. *Journal of Magnetic Resonance - Series B*, *111*(3), 209–219. https://doi.org/10.1006/jmrb.1996.0086

Beaulieu, C. (2002). The basis of anisotropic water diffusion in the nervous system - A technical review. In *NMR in Biomedicine* (Vol. 15, Issues 7–8, pp. 435–455). NMR Biomed. https://doi.org/10.1002/nbm.782

Benes, F. M. (1989). Myelination of cortical-hippocampal relays during late adolescence. *Schizophrenia Bulletin*, *15*(4), 585–593. https://doi.org/10.1093/schbul/15.4.585

Bezgin, G., Lewis, J. D., & Evans, A. C. (2018). Developmental changes of cortical white–gray contrast as predictors of autism diagnosis and severity. *Translational Psychiatry*, *8*(1), 249. https://doi.org/10.1038/s41398-018-0296-2

Bird, C. R., Hedberg, M., Drayer, B. P., Keller, P. J., Flom, R. A., & Hodak, J. A. (1989). MR assessment of myelination in infants and children: usefulness of marker sites. *American Journal of Neuroradiology*, *10*(4).

Brunsing, R. L., Schenker-Ahmed, N. M., White, N. S., Parsons, J. K., Kane, C., Kuperman, J., Bartsch, H., Kader, A. K., Rakow-Penner, R., Seibert, T. M., Margolis, D., Raman, S. S., McDonald, C. R., Farid, N., Kesari, S., Hansel, D., Shabaik, A., Dale, A. M., & Karow, D. S. (2017). Restriction spectrum imaging: An evolving imaging biomarker in prostate MRI. In *Journal of Magnetic Resonance Imaging* (Vol. 45, Issue 2, pp. 323–336). John Wiley and Sons Inc. https://doi.org/10.1002/jmri.25419

Casey, B. J., Cannonier, T., Conley, M. I., Cohen, A. O., Barch, D. M., Heitzeg, M. M., Soules, M. E., Teslovich, T., Dellarco, D. V, Garavan, H., Orr, C. A., Wager, T. D., Banich, M. T., Speer, N. K., Sutherland, M. T., Riedel, M. C., Dick, A. S., Bjork, J. M., Thomas, K. M., … Dale, A. M. (2018). The Adolescent Brain Cognitive Development (ABCD) study: Imaging acquisition across 21 sites. *Developmental Cognitive Neuroscience*, *32*, 43–54. https://doi.org/10.1016/J.DCN.2018.03.001

Casey, B. J., Jones, R. M., & Hare, T. A. (2008). The adolescent brain. In *Annals of the New York Academy of Sciences* (Vol. 1124, pp. 111–126). Blackwell Publishing Inc. https://doi.org/10.1196/annals.1440.010

Catani, M., Dell'Acqua, F., Vergani, F., Malik, F., Hodge, H., Roy, P., Valabregue, R., & Thiebaut de Schotten, M. (2012). Short frontal lobe connections of the human brain. *Cortex*, *48*(2), 273–291. https://doi.org/10.1016/j.cortex.2011.12.001

Chang, Y. S., Owen, J. P., Pojman, N. J., Thieu, T., Bukshpun, P., Wakahiro, M. L. J., Berman, J. I., Roberts, T. P. L., Nagarajan, S. S., Sherr, E. H., & Mukherjee, P. (2015). White matter changes of neurite density and fiber orientation dispersion during human brain maturation. *PLoS ONE*, *10*(6). https://doi.org/10.1371/journal.pone.0123656

Fischl, B., Salat, D. H., Busa, E., Albert, M., Dieterich, M., Haselgrove, C., Van Der Kouwe, A., Killiany, R., Kennedy, D., Klaveness, S., Montillo, A., Makris, N., Rosen, B., & Dale, A. M. (2002). Whole brain segmentation: Automated labeling of neuroanatomical structures in the human brain. *Neuron*, *33*(3), 341–355. https://doi.org/10.1016/S0896-6273(02)00569-X

Garavan, H., Bartsch, H., Conway, K., Decastro, A., Goldstein, R. Z., Heeringa, S., Jernigan, T., Potter, A., Thompson, W., & Zahs, D. (2018). Recruiting the ABCD sample: Design considerations and procedures. *Developmental Cognitive Neuroscience*, *32*, 16–22. https://doi.org/10.1016/j.dcn.2018.04.004

Geeraert, B. L., Lebel, R. M., & Lebel, C. (2019). A multiparametric analysis of white matter maturation during late childhood and adolescence. *Human Brain Mapping*, *40*(15), 4345–4356. https://doi.org/10.1002/hbm.24706

Genc, S., Malpas, C. B., Holland, S. K., Beare, R., & Silk, T. J. (2017). Neurite density index is sensitive to age related differences in the developing brain. *NeuroImage*, *148*, 373–380. https://doi.org/10.1016/j.neuroimage.2017.01.023

Genc, S., Seal, M. L., Dhollander, T., Malpas, C. B., Hazell, P., & Silk, T. J. (2017). White matter alterations at pubertal onset. *NeuroImage*, *156*, 286–292. https://doi.org/10.1016/j.neuroimage.2017.05.017

Genc, S., Smith, R. E., Malpas, C. B., Anderson, V., Nicholson, J. M., Efron, D., Sciberras, E., Seal, M. L., & Silk, T. J. (2018). Development of white matter fibre density and morphology over childhood: A longitudinal fixel-based analysis. *NeuroImage*, *183*, 666–676. https://doi.org/10.1016/j.neuroimage.2018.08.043

Grussu, F., Schneider, T., Tur, C., Yates, R. L., Tachrount, M., Ianuş, A., Yiannakas, M. C., Newcombe, J., Zhang, H., Alexander, D. C., DeLuca, G. C., & Gandini Wheeler-Kingshott, C. A. M. (2017). Neurite dispersion: a new marker of multiple sclerosis spinal cord pathology? *Annals of Clinical and Translational Neurology*, *4*(9), 663–679. https://doi.org/10.1002/acn3.445

Hagler, D. J., Ahmadi, M. E., Kuperman, J., Holland, D., McDonald, C. R., Halgren, E., & Dale, A. M. (2009). Automated white-matter tractography using a probabilistic diffusion tensor atlas: Application to temporal lobe epilepsy. *Human Brain Mapping*, *30*(5), 1535–1547. https://doi.org/10.1002/hbm.20619

Hagler, D. J., Hatton, S., Cornejo, M. D., Makowski, C., Fair, D. A., Dick, A. S., Sutherland, M. T., Casey, B. J., Barch, D. M., Harms, M. P., Watts, R., Bjork, J. M., Garavan, H. P., Hilmer, L., Pung, C. J., Sicat, C. S., Kuperman, J., Bartsch, H., Xue, F., … Dale, A. M. (2019). Image processing and analysis methods for the Adolescent Brain Cognitive Development Study. *NeuroImage*, 116091. https://doi.org/10.1016/J.NEUROIMAGE.2019.116091

Jernigan, T. L., Baaré, W. F. C., Stiles, J., & Madsen, K. S. (2011). Postnatal brain development. Structural imaging of dynamic neurodevelopmental processes. In *Progress in Brain Research* (Vol. 189, pp. 77–92). Elsevier B.V. https://doi.org/10.1016/B978-0-444-53884-0.00019-1

Jovicich, J., Czanner, S., Greve, D., Haley, E., van der Kouwe, A., Gollub, R., Kennedy, D., Schmitt, F., Brown, G., MacFall, J., Fischl, B., & Dale, A. (2006). Reliability in multi-site structural MRI studies: Effects of gradient non-linearity correction on phantom and human data. *NeuroImage*, *30*(2), 436–443. https://doi.org/10.1016/J.NEUROIMAGE.2005.09.046

Kaden, E., Kelm, N. D., Carson, R. P., Does, M. D., & Alexander, D. C. (2016). Multi-compartment

microscopic diffusion imaging. *NeuroImage*, *139*, 346–359. https://doi.org/10.1016/j.neuroimage.2016.06.002

Kinney, H. C., Brody, B. A., Kloman, A. S., & Gilles, F. H. (1988). Sequence of central nervous system myelination in human infancy: II. Patterns of myelination in autopsied infants. *Journal of Neuropathology and Experimental Neurology*, *47*(3), 217–234. https://doi.org/10.1097/00005072-198805000-00003

Krogsrud, S. K., Fjell, A. M., Tamnes, C. K., Grydeland, H., Mork, L., Due-Tønnessen, P., Bjørnerud, A., Sampaio-Baptista, C., Andersson, J., Johansen-Berg, H., & Walhovd, K. B. (2016a). Changes in white matter microstructure in the developing brain-A longitudinal diffusion tensor imaging study of children from 4 to 11years of age. *NeuroImage*, *124*, 473–486. https://doi.org/10.1016/j.neuroimage.2015.09.017

Krogsrud, S. K., Fjell, A. M., Tamnes, C. K., Grydeland, H., Mork, L., Due-Tønnessen, P., Bjørnerud, A., Sampaio-Baptista, C., Andersson, J., Johansen-Berg, H., & Walhovd, K. B. (2016b). Changes in white matter microstructure in the developing brain-A longitudinal diffusion tensor imaging study of children from 4 to 11years of age. *NeuroImage*, *124*(Pt A), 473–486. https://doi.org/10.1016/j.neuroimage.2015.09.017

Lebel, C., Walker, L., Leemans, A., Phillips, L., & Beaulieu, C. (2008). Microstructural maturation of the human brain from childhood to adulthood. *NeuroImage*, *40*(3), 1044–1055. https://doi.org/10.1016/j.neuroimage.2007.12.053

Lebel, Catherine, & Beaulieu, C. (2011a). Longitudinal development of human brain wiring continues from childhood into adulthood. *Journal of Neuroscience*, *31*(30), 10937–10947. https://doi.org/10.1523/JNEUROSCI.5302-10.2011

Lebel, Catherine, & Beaulieu, C. (2011b). Longitudinal development of human brain wiring continues from childhood into adulthood. *Journal of Neuroscience*, *31*(30), 10937–10947. https://doi.org/10.1523/JNEUROSCI.5302-10.2011

Lewis, J. D., Evans, A. C., & Tohka, J. (2018). T1 white/gray contrast as a predictor of chronological age, and an index of cognitive performance. *NeuroImage*, *173*, 341–350. https://doi.org/10.1016/j.neuroimage.2018.02.050

Lynch, K. M., Cabeen, R. P., Toga, A. W., & Clark, K. A. (2020). Magnitude and timing of major white matter tract maturation from infancy through adolescence with NODDI. *NeuroImage*, *212*, 116672. https://doi.org/10.1016/j.neuroimage.2020.116672

Mah, A., Geeraert, B., & Lebel, C. (2017). Detailing neuroanatomical development in late childhood and early adolescence using NODDI. *PLOS ONE*, *12*(8), e0182340. https://doi.org/10.1371/journal.pone.0182340

Menon, V., & Uddin, L. Q. (2010). Saliency, switching, attention and control: a network model of insula function. *Brain Structure and Function*, *214*(5–6), 655–667. https://doi.org/10.1007/s00429-010-0262-0

Morrell, C. H., Brant, L. J., & Ferrucci, L. (2009). Model choice can obscure results in longitudinal studies. *Journals of Gerontology - Series A Biological Sciences and Medical Sciences*, *64*(2), 215–222. https://doi.org/10.1093/gerona/gln024

Moura, L. M., Kempton, M., Barker, G., Salum, G., Gadelha, A., Pan, P. M., Hoexter, M., Del Aquilla, M. A. G., Picon, F. A., Anés, M., Otaduy, M. C. G., Amaro, E., Rohde, L. A., McGuire, P., Bressan, R. A., Sato, J. R., & Jackowski, A. P. (2016). Age-effects in white matter using associated diffusion tensor imaging and magnetization transfer ratio during late childhood and early adolescence. *Magnetic Resonance Imaging*, *34*(4), 529–534. https://doi.org/10.1016/j.mri.2015.12.021

Mukherjee, P., Berman, J. I., Chung, S. W., Hess, C. P., & Henry, R. G. (2008). Diffusion tensor MR

imaging and fiber tractography: Theoretic underpinnings. In *American Journal of Neuroradiology* (Vol. 29, Issue 4, pp. 632–641). American Journal of Neuroradiology. https://doi.org/10.3174/ajnr.A1051

Ouyang, M., Kang, H., Detre, J. A., Roberts, T. P. L., & Huang, H. (2017). Short-range connections in the developmental connectome during typical and atypical brain maturation. In *Neuroscience and Biobehavioral Reviews* (Vol. 83, pp. 109–122). Elsevier Ltd. https://doi.org/10.1016/j.neubiorev.2017.10.007

Pangelinan, M. M., Leonard, G., Perron, M., Pike, G. B., Richer, L., Veillette, S., Pausova, Z., & Paus, T. (2016). Puberty and testosterone shape the corticospinal tract during male adolescence. *Brain Structure and Function*, *221*(2), 1083–1094. https://doi.org/10.1007/s00429-014-0956-9

Peters, B. D., Szeszko, P. R., Radua, J., Ikuta, T., Gruner, P., Derosse, P., Zhang, J. P., Giorgio, A., Qiu, D., Tapert, S. F., Brauer, J., Asato, M. R., Khong, P. L., James, A. C., Gallego, J. A., & Malhotra, A. K. (2012). White matter development in adolescence: Diffusion tensor imaging and meta-analytic results. *Schizophrenia Bulletin*, *38*(6), 1308–1317. https://doi.org/10.1093/schbul/sbs054

Pohl, K. M., Sullivan, E. V., Rohlfing, T., Chu, W., Kwon, D., Nichols, B. N., Zhang, Y., Brown, S. A., Tapert, S. F., Cummins, K., Thompson, W. K., Brumback, T., Colrain, I. M., Baker, F. C., Prouty, D., De Bellis, M. D., Voyvodic, J. T., Clark, D. B., Schirda, C., … Pfefferbaum, A. (2016). Harmonizing DTI measurements across scanners to examine the development of white matter microstructure in 803 adolescents of the NCANDA study. *NeuroImage*, *130*, 194–213. https://doi.org/10.1016/j.neuroimage.2016.01.061

Simmonds, D. J., Hallquist, M. N., Asato, M., & Luna, B. (2014). Developmental stages and sex differences of white matter and behavioral development through adolescence: A longitudinal diffusion tensor imaging (DTI) study. *NeuroImage*, *92*, 356–368. https://doi.org/10.1016/j.neuroimage.2013.12.044

Song, S. K., Yoshino, J., Le, T. Q., Lin, S. J., Sun, S. W., Cross, A. H., & Armstrong, R. C. (2005). Demyelination increases radial diffusivity in corpus callosum of mouse brain. *NeuroImage*, *26*(1), 132–140. https://doi.org/10.1016/j.neuroimage.2005.01.028

Sørensen, Ø., Walhovd, K. B., & Fjell, A. M. (2021). A recipe for accurate estimation of lifespan brain trajectories, distinguishing longitudinal and cohort effects. *NeuroImage*, *226*. https://doi.org/10.1016/j.neuroimage.2020.117596

Tamnes, C. K., Østby, Y., Fjell, A. M., Westlye, L. T., Due-Tønnessen, P., & Walhovd, K. B. (2010). Brain maturation in adolescence and young adulthood: Regional age-related changes in cortical thickness and white matter volume and microstructure. *Cerebral Cortex*, *20*(3), 534–548. https://doi.org/10.1093/cercor/bhp118

Tusa, R. J., & Ungerleider, L. G. (1985). The inferior longitudinal fasciculus: A reexamination in humans and monkeys. *Annals of Neurology*, *18*(5), 583–591. https://doi.org/10.1002/ana.410180512

Uddin, L. Q., Nomi, J. S., Hébert-Seropian, B., Ghaziri, J., & Boucher, O. (2017). Structure and Function of the Human Insula. In *Journal of Clinical Neurophysiology* (Vol. 34, Issue 4, pp. 300–306). Lippincott Williams and Wilkins. https://doi.org/10.1097/WNP.0000000000000377

Wald, L., Schmitt, F., & Dale, A. (2001). Systematic spatial distortion in MRI due to gradient non-linearities. *NeuroImage*, *13*(6), 50. https://doi.org/10.1016/s1053-8119(01)91393-x

Wells, W. M., Viola, P., Atsumi, H., Nakajima, S., & Kikinis, R. (1996). Multi-modal volume registration by maximization of mutual information. *Medical Image Analysis*, *1*(1), 35–51. https://doi.org/10.1016/S1361-8415(01)80004-9

White, N. S., Leergaard, T. B., D'Arceuil, H., Bjaalie, J. G., & Dale, A. M. (2013). Probing tissue microstructure with restriction spectrum imaging: Histological and theoretical validation. *Human*

*Brain Mapping*, *34*(2), 327–346. https://doi.org/10.1002/hbm.21454

White, N. S., McDonald, C. R., Farid, N., Kuperman, J., Karow, D., Schenker-Ahmed, N. M., Bartsch, H., Rakow-Penner, R., Holland, D., Shabaik, A., Bjørnerud, A., Hope, T., Hattangadi-Gluth, J., Liss, M., Parsons, J. K., Chen, C. C., Raman, S., Margolis, D., Reiter, R. E., … Dale, A. M. (2014). Diffusion-weighted imaging in cancer: Physical foundations and applications of restriction spectrum imaging. In *Cancer Research* (Vol. 74, Issue 17, pp. 4638–4652). American Association for Cancer Research Inc. https://doi.org/10.1158/0008-5472.CAN-13-3534

Yakovlev, P., & Lecours, A. (1967). *The myelogenetic cycles of regional maturation of the brain. In: Resional development of the brain in early life*. http://www.sciepub.com/reference/145890

Zhuang, J., Hrabe, J., Kangarlu, A., Xu, D., Bansal, R., Branch, C. A., & Peterson, B. S. (2006). Correction of eddy-current distortions in diffusion tensor images using the known directions and strengths of diffusion gradients. *Journal of Magnetic Resonance Imaging*, *24*(5), 1188–1193. https://doi.org/10.1002/jmri.20727